International journal of innovation in Engineering

journal homepage: www.ijie.ir

Research Paper

Absorption in the wavemaker by Artificial neural networks (ANNs)

Meysam Amini[a1], **Mohammad Saeed Seif**[b]

[a] *PhD Candidate, Faculty of Management, University of Tehran, Tehran, Iran; Emil Address; meysam.amini@ut.ac.ir*

[b] *Professor of Department Of Mechanical Engineering, Sharif University of Technology, Tehran, Iran; Emil Address; seif@sharif.edu*

ARTICLE INFO

Received: 06 January 2022

Reviewed: 18 January 2022

Revised: 01 February 2022

Accepted: 12 February 2022

Keywords:

Absorption, Wave Maker, Artificial Neural Networks

ABSTRACT

Wave-making theories are becoming available, but their applicability is limited to specific ranges of waves and wavemaker types. Machine learning can also be used to discover nonlinear functional relationships. As a result, based on machine learning, this paper proposes a simple and universal framework for generating and absorbing waves. This framework trains neural networks to determine the transfer function between the wavemaker's free-surface elevation and velocity. To increase the generalization ability of neural networks, penalty term and data augmentation techniques based on wave-making mechanisms are introduced, rather than pure data-driven. As a result, once the wavemaker has the target wave profiles in front of it, it can generate waves while also absorbing reflected waves. Analytical solutions are used to validate the simulated wave profiles and wave orbital velocities, demonstrating that the proposed framework is effective at eliminating the re-reflection wave. The validation for generating the solitary wave and the New Year's wave is then performed, indicating that the generated waves agree very well with the desired wave elevation. The proposed framework can help with wavemaker design in the future, and it does not require any complex theoretical derivation.

1. Introduction

A wavemaker is usually installed at one end of a hydraulic flume to generate two-dimensional wave trains. They generate waves by relating the wavemaker stroke to wave elevation using linear transfer functions, but the initial linear waves must travel a certain distance before evolving to the desired nonlinear waves. Meanwhile, a common technique for reducing reflections from the flume's end wall is to construct a dissipative beach with a constant slope in front of the end wall. It will, however, increase the length of the flume's non-test domain.

[1] **Corresponding Author**
meysam.amini@ut.ac.ir

If waves interacting with coastal or offshore structures are studied, the dissipative beach cannot eliminate any waves reflecting to the wave maker. As a result, the active wave absorption system is required. Early works on active absorbing waves used digital filters or linear transfer functions that related the wavemaker stroke to wave elevation (Schäffer and Klopman, 2000).

However, the implementation of these methods is complex and difficult to make universal for wavemakers of arbitrary shapes, and they are unable to take advantage of data fusion techniques.To that end, this paper proposes a machine-learning-based universal method for active wave generation and absorption.

The goal of this method is to directly train neural networks to represent transfer functions that map the desired surface-elevation at a front-mounted wave gauge to the wavemaker motion required to create it, which is applicable to wavemakers of any shape. When creating waves with absorbing wavemakers, the wavemaker movement is controlled to generate the desired incident waves while also absorbing reflected waves. The control signal can be obtained by transforming the wave signal in time with a time-domain or frequency-domain filter. Hirakuchi et al. (1990) created a piston-type absorbing wavemaker that used the water surface elevation at the paddle's mean position as hydraulic feedback. Spinneken and Swan (2009) presented a mathematical model for an absorbing wavemaker, as well as experimental verification, based on force-feedback control. Christensen and Frigaard (1995) proposed an active absorption system based on free-surface elevation and orbital velocities at a fixed position in the fluid domain, using digital filters to estimate the absorption transfer function. Schäffer and Jakobsen (2003) also developed a method for fitting the frequency response of a digital filter to approximate the absorption transfer function using linear theory, but the fitting technique was not discussed. Yang et al. (2016) used an infinite impulse response digital filter to approximate the absorption transfer function using the iterative reweighted least-squares algorithm based on first order wavemaker theory. Even though the preceding literature review introduces some previous works on active absorbing wavemakers, the majority of researchers focused on the active absorption system in the frequency domain. Schaffer and Klopman (2000) proposed a simple active wave absorption system based on free-surface elevation measured at the wavemaker in time-domain active absorption techniques, with the general assumption being linear long-crested wave theory in shallow water.

However, analytical solutions for wave generation are still difficult to obtain for plunger-type wave makers. The efficiency of the plunger-type wavemaker in deep water is higher than that of the piston due to the shape of the plunger-type wavemaker more closely matching the velocity profile of near-surface water waves (Timmerberg et al., 2015). Wu (1988) established the transfer function for relating the plunger-type wavemaker's stroke amplitude to the far-field wave amplitude as a function of wavenumber using the boundary element method (BEM). He et al. (2021) proposed a theoretical method for generating solitary waves with plungers and specified its constraints on the produced wave height. However, if the plunger shape is changed or an unusual shape is given, the formulae must be deduced again or even have no solution, especially when the gap is considered (Wu, 1991; Nikseresht & Bingham, 2020). As a result, further advancements are required to create control signals for plunger-type devices using optimization procedures or nonlinear transfer functions (Hicks et al., 2021). The wave-making system proposed in this paper can easily map nonlinear transfer functions, extending the functionality of existing plunger-type wave makers.

Most researchers focused on linear theory methods (Schaffer and Klopman, 2000; Didier and Neves, 2012; Szmelter-Jarosz et al., 2021) or infinite impulse response digital filter methods (Yang et al., 2016; De Mello et al., 2017; Spinneken and Swan, 2012) to establish transfer functions relating wavemaker velocity to desired free-surface elevation in front of the wavemaker. Nonlinear wave generation, on the other hand, necessitates high-order wave-making theory, and there is limited evidence of analytical solutions encompassing all features relevant in the applied ocean, as well as coastal research (Eldrup et al., 2019; Khait & Shemer, 2019). Mahjouri et al. (2020) recently proposed a simple and practical active control algorithm for piston-type wavemakers using constant gains.

Even though no transfer function or filter was used in the feedback and feed-forward loops of the control system, the constant gains must be adjusted in each test where the water depth and working frequency change. The above-mentioned methods' implementation may be complex and difficult to be universal for arbitrary wavemakers. As a result, this work focuses on machine learning methods with strong nonlinear mapping capability. Machine learning has gotten a lot of attention in the field of fluid mechanics in recent years (Chen et al., 2021; Lee et al., 2019). The artificial neural network (ANN), which is represented as a set of interconnected neurons, is one of the most widely used structures in machine learning methods. These neurons function numerically, with sequential multiplication accumulation operations connecting them. Schmitt implemented the use of neural networks to predict wavemaker inputs based on specific wave traces for the calibration of waves near the breaking limit. Their findings suggest that neural networks are a useful tool for calibrating wavemakers and that more experiments will yield better results.

To the best of our knowledge, no systematic study has been conducted to establish a universal framework for mapping the absorption transfer function relating the wavemaker velocity to the desired free-surface elevation in front of the wavemaker by ANNs. To that end, the central goal of this work is to introduce the ANN-mapped transfer function in our numerical wave flume, including data generation, data augmentation technology, and hyper-parameters sensitivity analysis during the training process. The following is how the work progresses. For model training, waves are first generated by the wavemaker's sinusoidal motion. The monitored surface elevations were then used as model input, with the given wavemaker velocity as the desired model output. More data is available as different sinusoidal motions of the wavemaker are run, and the model's generalization ability improves. The wavemaker velocity will then be adjusted to match the velocity induced by the waves that must be absorbed in practice. This wave absorption system has two distinct advantages. For starters, arbitrary shape wavemakers can be used to quickly apply a wide range of wave conditions. Second, the transfer function needed to absorb reflecting waves can also be used to generate a given wave.

2. Numerical Method

The numerical method used for an in-house developed CFD solver, including the Navier-Stokes equation solver and level set method, is introduced in this section.

2.1. Navier-Stokes Equation Solve

Based on the finite difference method, an in-house developed CFD solver is established. The Navier-Stokes equations for incompressible and viscous fluids are written as:

$$\nabla . u = 0 \tag{1}$$

$$\frac{\partial u}{\partial t} + (u.\nabla).u = -\frac{1}{\rho}\nabla p + \frac{\mu}{\rho}\nabla^2 u + g \tag{2}$$

where u is the velocity vector, p is the pressure, and g is the gravitational acceleration. ρ and μ denote the density and viscosity, respectively.

To solve the Navier-Stokes equations, the prediction-correction fractional steps solution scheme (Chorin, 1968) is used, and mass conservation is achieved by coupling the pressure term with the continuity equation. The pressure term is then decoupled from the momentum equation using an intermediate velocity term. The velocity field and pressure field of the fluid at the next moment can be calculated using the non-incremental pressure correction. A third-order finite-difference scheme, Cubic Interpolated Pseudo particle (CIP), is used to calculate the advection term in Eq. (2). (Yabe et al., 2001). The central difference method is used to calculate the second part of the non-advection term in Eq. (2). An algebraic multigrid solver is used to solve the pressure Poisson equation. To deal with the fluid-solid interaction, the ghost-node immersed boundary

method (Peskin, 2002; Calderer et al., 2014) is used in this study. The ghost nodes are used to demonstrate the effect of the moving body.

2.2. Method of Establishing Levels

The level set method has been widely used to calculate free surface flows as a front capturing technique for interfaces (Osher and Fedkiw, 2001; Osher, et al., 2004). The level set method is based on forming a high-dimensional function to handle topological changes, and then viewing the interface as the function's zero level sets. The transport of the level set function under a given velocity field can be regarded as solving the advection equation. The semi-Lagrangian scheme is used in this study to solve the advection equation of the level set function, which has good stability (van Leer, 1979). The level set function (X,t) is a signed function, with the liquid phase being positive and the gas phase being negative. The interface can be written as:

$$\Gamma = \{X|\Phi(x,t) = 0\} \tag{3}$$

$$\Phi(x,t=0) = \begin{cases} d(X,\Gamma)\ for\ X\ in\ the\ liqouid \\ 0\ for\ X \in \Gamma \\ -d(X,\Gamma)\ for\ X\ in\ the\ gas, \end{cases} \tag{4}$$

$d(X,\Gamma)$ denotes the distance function. depending on the sign of $\Phi(x,t)$, the density and viscosity of each fluid can take on two different values, which can be expressed as:

$$\rho(\overline{\Phi}) = \rho_G + (\rho_L - \rho_G)\overline{H}(\overline{\Phi}) \tag{5}$$

$$\mu(\overline{\Phi}) = \mu_G + (\mu_L - \mu_G)\overline{H}(\overline{\Phi}) \tag{6}$$

where G and L represent the gas and liquid phases, respectively

3. ANN-based Wave Generation Methodology

In this study, we directly establish the transfer function between the wavemaker velocity and the free-surface elevation in front of the wavemaker. As a result, once we have the target wave profiles in front of the wavemaker, we can generate waves while also absorbing reflected waves. The target waves can be generated close to the wavemaker, eliminating the need for long-distance propagation, and potentially shortening the flume's length. The numerical wave flume is used in this paper to prepare suitable training data, but the method should be applicable to any numerical and physical wavemaker.

3.1. General Framework

The problem of determining the transfer function can be illustrated in the following way, according to Schmitt et al. (2021). To begin, we have an output variable Vp_i, the required wavemaker velocity, defined as a function $F(\mu_i, V\mu_i \dots W_i)$ that is affected by hydraulic feedbacks such as free-surface elevation in front of the wavemaker and some wave parameters. We can obtain a set of vectors S_i by forcing sinusoidal motion of the wavemaker, which represents the set of observations $(\mu_i, V\mu_i \dots W_i)$ at the probe mounted in front of the wavemaker. The inputs and output scan be defined by Eq. (7)

$$F(S(\mu, V_\mu, \dots, W) \rightarrow V_p \tag{7}$$

Then, using neural networks' universal approximation feature, we can find an approximation for the unknown function F by associating the variable Vp_i with the vectors S_i from a series of collected samples. The proposed framework's block diagram is depicted in Fig. 1. The measured free-surface elevation μ_m in the main control loop includes the generated, reflected, and re-reflected waves. A data file containing the desired free-surface elevation μ_d is provided. As a result, the reflected wave free-surface elevation,μ_R , is to be absorbed by comparing the desired free-surface elevation, μ_d, with the measured one in front of the wavemaker, μ_m. The wavemaker velocity will then take into account the velocity induced by the wave that

will be absorbed. The feedback signal consists of the measured free-surface elevation μ_m, the desired free-surface elevation μ_d, the position of the wavemaker, and the wave parameters. The wavemaker elevation control is analogous to the wavemaker velocity control.

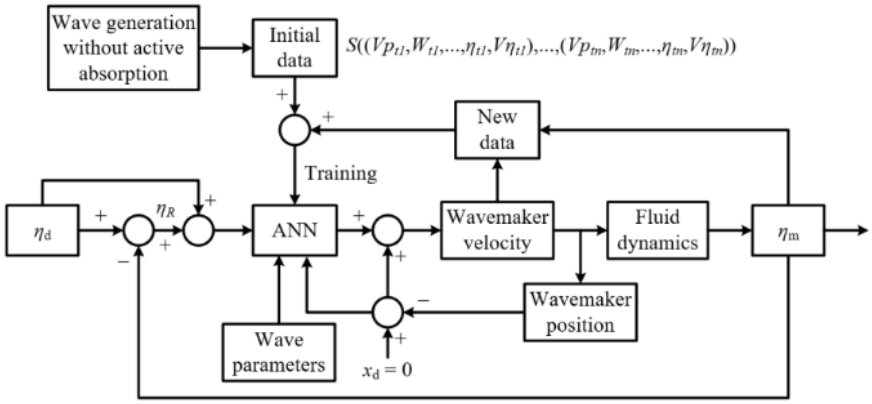

Fig. 1. Diagram of the absorbing wavemaker framework

However, it should be noted that controlling the wavemaker velocity does not necessarily guarantee the position control of the wavemaker. Possible drift in the position of the wavemaker may saturate the wavemaker stroke during the wave elevation control. To prevent this drift, closed-loop position control of the wavemaker is employed. This action needs to be slow and smooth enough to avoid any disturbance of the wave absorption loop. The initial zero-position '$x_d = 0$' is used as the desired input and a smoother transition (e.g. a power function) is used to regulate the wavemaker.

3.2. Structure of ANNs

The multi-layer perceptron (MLP) model is utilized for the structure of ANNs. If the activation function is continuous, bounded and non-constant, the multi-layer feed-forward neural network can approximate any well-behaved function (Hornik, 1991). Once trained, any required free-surface elevation in front of the wavemaker can be generated without further iterative calibration steps. The detailed structure of the ANNs is illustrated in Fig. 2. The input variables mean the observations $(\mu_i, V\mu_i \ldots W_i)$. The left scatter plots of Fig.2 present a series of collected samples. The input variables include surface elevation at the wave gauge and other monitor parameters. The output variable is the required wavemaker velocity. For the training of the ANNs, the initial process is forcing the sinusoidal motion of the wavemaker to generate a series of regular waves. Of course, forcing the random motion of the wavemaker to generate a series of irregular waves is also acceptable. The transfer function is then trained by relating the wavemaker velocity to the measured observations.

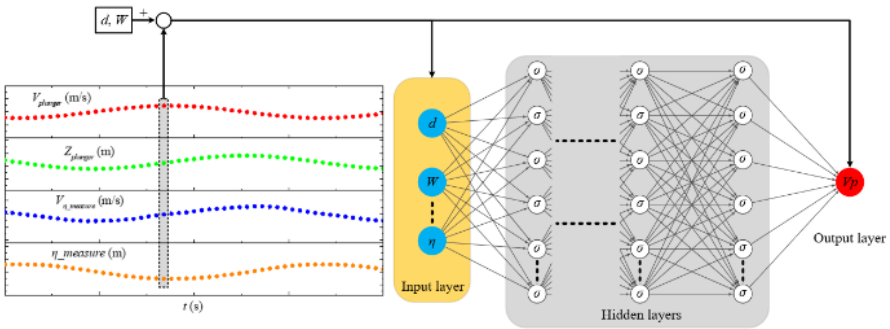

Fig. 2. Structure of the ANNs. The left scatter plots present an example of a sample set.

The input variables include surface elevation at the wave gauge and other monitor parameters. The output variable is the required wavemaker

4. Absorbing Wavemaker (piston type)

The piston-type wavemaker is tested in this section, data generation for the training of the ANNs will be given in subsection 4.1. Then, the influence of the hyper-parameters on the mapping accuracy will be discussed in subsection 4.2. In subsection 4.3, regular wave generation with active wave absorption for full reflection case (i.e. a standing monochromatic wave) will be tested.

4.1. 4.1 Data Generation

In this section, the wave is generated without active absorption with a damping region at the end of the wave flume to ensure that the training set is free of wave reflection interference. Fig.3 depicts the 2D numerical wave flume diagram. The depth of the still water is d, and the length of the flume is $12L$, where L is the characteristic wavelength. The paddle's initial zero-position is located at $x = 0\,m$. Wave damping zones with a width of $6L$ are installed on the right sides of the flume. A non-uniform grid distribution is used to discretize the entire computational domain. In this study, the numerical time step dt is $1.0 \times 10^{-3} s$.

The free-surface elevation is measured using a wave gauge mounted in front of the wavemaker. Multiple distinct instances of the input and output variables can be recorded to generate enough data for neural network model training by forcing the sinusoidal motion of the wavemaker to generate a series of regular waves. The cases for data generation can be arbitrary (forcing random motion of the wavemaker to generate a series of irregular waves is also acceptable), if their range covers the target wave's period and wave height. The sinusoidal motion of the wavemaker is selected here, and the motion parameters are listed in Table 1. Each case only requires about three periods of the wavemaker's sinusoidal motion. It should be noted that the input variables defined in this section are simply the free-surface elevation in front of the wavemaker, the wave period (peak wave period for irregular waves), and the water depth.

Table 1. The Sinusodial Motion Parameters for Data Generation

		T=0.8 s	*T*=1.0 s	*T*=1.2 s	*T*=1.4 s
d=0.4 m	Stroke=0.04 m	Case1	Case2	Case3	Case4
	Stroke=0.08 m	Case5	Case6	Case7	Case8
	Stroke=0.12 m	Case9	Case10	Case11	Case12
d=0.5 m	Stroke=0.04 m	Case13	Case14	Case15	Case16
	Stroke=0.08 m	Case17	Case18	Case19	Case20
	Stroke=0.12 m	Case21	Case22	Case23	Case24
d=0.6 m	Stroke=0.04 m	Case25	Case26	Case27	Case28
	Stroke=0.08 m	Case29	Case30	Case31	Case32
	Stroke=0.12 m	Case33	Case34	Case35	Case36

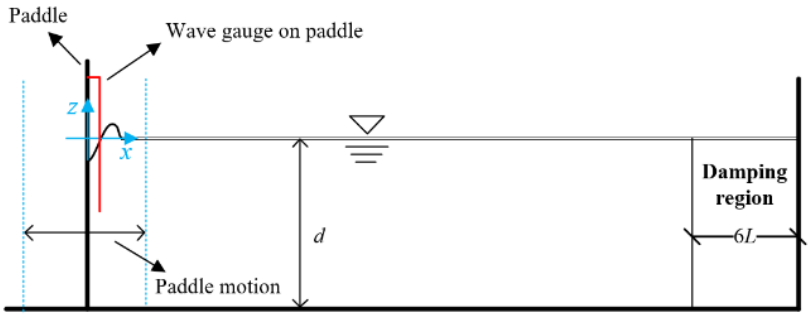

Fig. 3. Schematics of the 2D numerical wave flume

4.2. Influence of the Hyper-Parameters on the Mapping Accuracy

The hyper-parameters in an MLP model can affect the mapping accuracy. Here, we will discuss the number of layers used, the number of neurons per layer, the ratio of dropout layer (Srivastava et al., 2014) and the penalty term. The dropout layer is used to prevent neural networks from overfitting. The loss function used in the training process is defined as Eq. (8) where the second term of the left side is the penalty term. The penalty term is first proposed in this study to embed the physical feature into the MLP model and prevent neural networks from overfitting, which means that the wavemaker velocity and the free-surface elevation should be in the opposite direction.

$$Loss = \sum_{n=1}^{N} |Vp(S_n)_{ANN} - Vp_n|^2 + \lambda \sum_{n=1}^{N} |sing(Vp(S_n)_{ANN}) + sign(\eta_n)|^2 \quad (8)$$

$$MSE = \sum_{n=1}^{N} \left| ||Vp(S_n)_{ANN} - Vp_n|| \right|^2 \quad (6)$$

In this study, the activation function used at each layer is chosen as Rectified Linear (ReLU). The k-fold cross-validation is usually used to eliminate the bias in the training data. Therefore, the data samples will be divided in a 9:1 ratio of training to test samples and then the members of each set are chosen randomly. In this study, the mean of squares of errors (MSE) between the samples and the predictions during the training phase is used as the judgment criterion of mapping accuracy, shown in Eq. (9).

The basic values of these hyper-parameters are selected as that the number of layers is 4, the number of neurons per layer is 32, the ratio of dropout layer is 10% and the weight of the penalty term λ is 1. The training epoch is fixed at 2400. Table 2 shows the test results of hidden layer parameters including the number of layers and the number of neurons per layer. As expected, we observe that as the number of layers and neurons is increased (e.g the capacity of the neural network to approximate more complex functions), the predictive accuracy is increased. The results showed that all tasks convergence with a MSE below 0.0001.

Table 2. MSE of the Test for the Hidden Layer Parameters

	Neurons =16	Neurons =32	Neurons =64
Layers=2	5.39038e-05	2.02104e-05	8.07028e-06
Layers=4	4.13974e-05	1.75347e-05	6.85055e-06
Layers=6	3.87137e-05	1.67195e-05	6.08309e-06

Table 3. MSE of the Test for the Overfiying Parameters

	Dropout =0	Dropout =10	Dropout =20
Weight λ =0	5.17951e-05	2.17839e-05	1.33114e-05
Weight λ =1	3.12597e-05	1.75347e-05	4.89697e-06
Weight λ =5	2.17839e-05	3.88151e-06	3.53083e-06

Table 3 shows the test results of the overfitting prevention parameters including the ratio of dropout layer and the weight of the penalty term λ. The results showed that as the ratio of the dropout layer and the weight of the penalty term are increased, the predictive accuracy is increased. The proposed penalty term in this study has played a positive role.

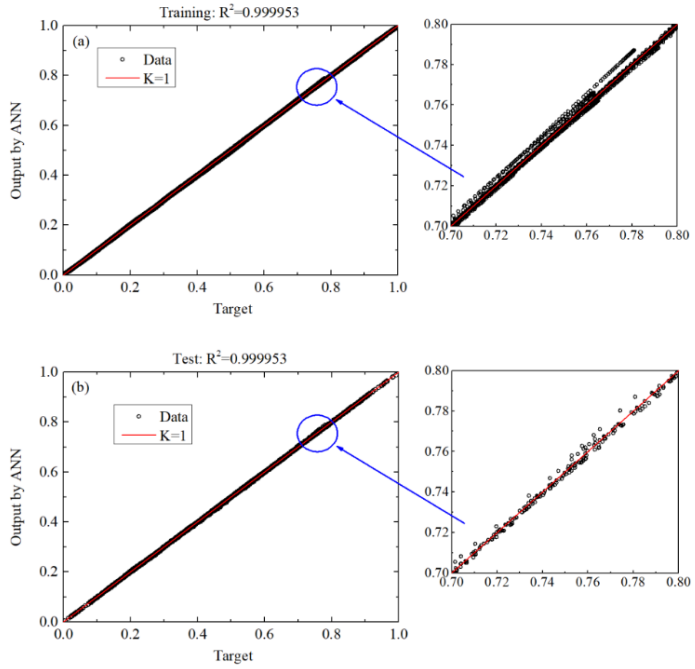

Fig. 4 The scatter plot of the estimated and the observed values of the normalized V_p.

Based on the above analysis, we identified the parameters ultimately used for subsequent studies that the number of layers is 6, the number of neurons per layer is 64, the ratio of dropout layer is 20% and the weight of the penalty term λ is 5. Fig. 4 shows the scatter plot of the estimated (outputs by ANN) and the observed (samples) values of the normalized Vp. If the fit were perfect, all the points should lie on the 45-degree line K. Fig. 4(a) shows the fit for the training data while Fig. 4(b) shows the same thing for the test data. The MPL model performs very well.

4.3. Testing the Learned ANN on Absorbing Wave Making

The performance of the proposed wave-making system in eliminating spurious re-reflection of outgoing waves is demonstrated in this section. In this case, monochromatic wave generation with active wave absorption is expected to produce a standing wave in the computational domain. Figure 5 depicts the 2D numerical wave flume diagram. The wavemaker is located at one end, and the wall is 8L away from it. The wavemaker's targeting incident wave is a second-order Stokes wave. The incident wave has a period of 0.851 seconds and an amplitude of 0.018 m. To record the wave evolution, two wave gauges, WG1 and WG2, are

used, which are located at the antinode (equal to L/2 from the right-side wall) and node (equal to L/4 from the right-side wall), respectively.

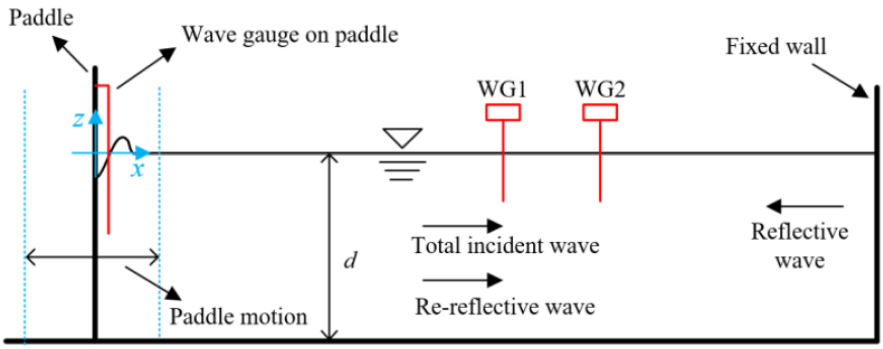

Fig. 5 Schematics of the 2D numerical wave flume

The time series of free-surface elevation at node and antinode is shown in Fig. 6. For comparison, the target solutions (i.e. second-order Stokes solutions) are also plotted, assuming perfect reflection at the right-side wall. It is well understood that a perfect active wave absorption system can completely absorb the reflected wave energy and then prevent the incident wave from diverging. The amplitudes at the node are very small, and the amplitudes at the antinode are in good agreement with the expected second-order solution, as shown in Fig. 6, demonstrating the capability of the proposed wave-making system.

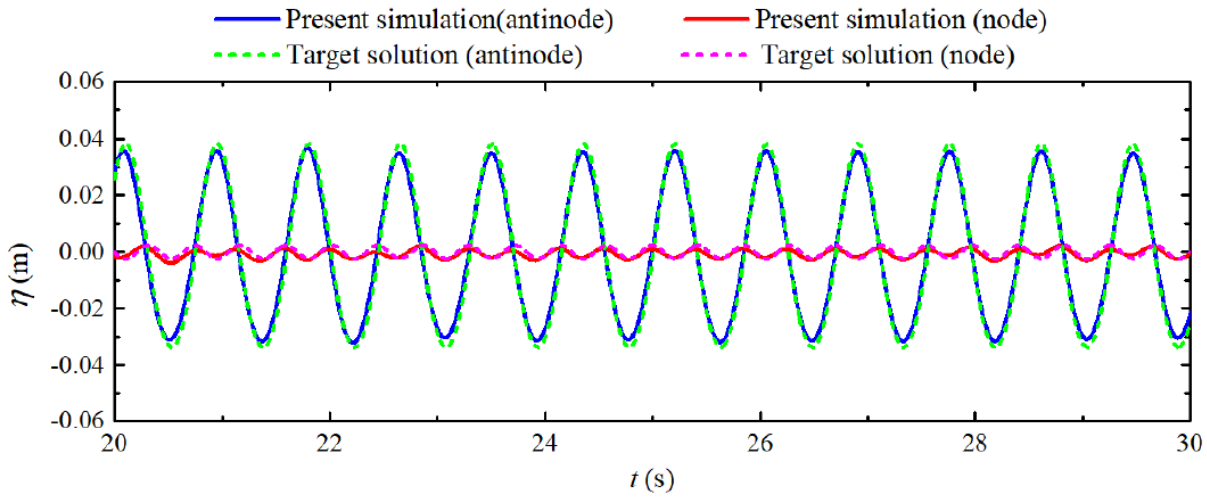

Fig. 6 Time series of the free-surface elevation at node and antinode

5. Conclusion

A universal framework for wavemakers with a front-mounted wave gauge to generate and absorb waves is proposed in this paper. The neural networks are trained to determine the transfer function between the wavemaker's free-surface elevation and velocity. Once the wavemaker has the target wave profiles in front of it, it can generate waves while also absorbing reflected waves. The penalty term is used to incorporate the physical feature into the loss function and prevent neural networks from becoming overfit.

The following are the main conclusions:

The convergence error is reduced and the error distribution is more concentrated near zero error when data augmentation is used to enrich the input variables. From the standpoint of wave-making mechanisms, the variable of free-surface elevation velocities increases momentum information, whereas the couple of free-

surface elevation in front of the wavemaker and the position of the wavemaker provide information on waterplane area. In the case of regular waves with full reflection, it is shown that the proposed framework can effectively absorb re-reflection waves and produce pure standing waves. Given the target wave profiles in front of the wavemaker, it is possible to generate the desired wave-elevation time series for New-year waves and solitary waves. This study demonstrates the utility of machine learning technology in the generation and absorption of waves.

Further research and development should be carried out in order to apply this method to practical experiments and improve the technology's utilization. Using piston and plunger wavemakers as examples, an in-house numerical solver simulates both wave generation and absorption.

References

- Calderer, A., Kang, S., & Sotiropoulos, F. (2014). Level set immersed boundary method for coupled simulation of air/water interaction with complex floating structures. Journal of Computational Physics, 277, 201-227.
- Chen, H., Fu, Q., Liao, Q., Zhu, X., & Shah, A. (2021). Applying artificial neural network to predict the viscosity of microalgae slurry in hydrothermal hydrolysis process. Energy and AI, 4, 100053.
- de Mello, D. P., de Freitas, M. L., Cordeiro, L. C., Júnior, W. S., de Bessa, I. V., & Clavier, L. (2017). Verification of Magnitude and Phase Responses in Fixed-Point Digital Filters. arXiv preprint arXiv:1706.05088.
- Didier, E., & Neves, M. G. (2012). A semi-infinite numerical wave flume using Smoothed Particle Hydrodynamics. International Journal of Offshore and Polar Engineering, 22(03).
- Eldrup, M. R., & Lykke Andersen, T. (2019). Applicability of nonlinear wavemaker theory. Journal of Marine Science and Engineering, 7(1), 14.
- Frigaard, P., & Christensen, M. (1995). An absorbing wave-maker based on digital filters. In Coastal Engineering 1994 (pp. 168-180).
- He, M., Khayyer, A., Gao, X., Xu, W., & Liu, B. (2021). Theoretical method for generating solitary waves using plunger-type wavemakers and its Smoothed Particle Hydrodynamics validation. Applied Ocean Research, 106, 102414.
- Hirakuchi, H., Kajima, R., & Kawaguchi, T. (1990). Application of a piston-type absorbing wavemaker to irregular wave experiments. Coastal Engineering in Japan, 33(1), 11-24.
- Khait, A., & Shemer, L. (2019). Nonlinear wave generation by a wavemaker in deep to intermediate water depth. Ocean Engineering, 182, 222-234.
- Lee, S., Lee, K. K., & Yoon, H. (2019). Using artificial neural network models for groundwater level forecasting and assessment of the relative impacts of influencing factors. Hydrogeology Journal, 27(2), 567-579.
- Mahjouri, S., Shabani, R., Rezazadeh, G., & Badiei, P. (2020). Active control of a piston-type absorbing wavemaker with fully reflective structure. China Ocean Engineering, 34(5), 730-737.
- Nikseresht, A. H., & Bingham, H. B. (2020). A Numerical Investigation of Gap and Shape Effects on a 2D Plunger-Type Wave Maker. Journal of Marine Science and Application, 19(1), 101-115.
- Osher, S., & Fedkiw, R. P. (2001). Level set methods: an overview and some recent results. Journal of Computational physics, 169(2), 463-502.
- Osher, S., Fedkiw, R., & Piechor, K. (2004). Level set methods and dynamic implicit surfaces. Appl. Mech. Rev., 57(3), B15-B15.
- Peskin, C. S. (2002). The immersed boundary method. Acta numerica, 11, 479-517.

- Schäffer, H. A., & Jakobsen, K. P. (2003, August). Non-linear wave generation and active absorption in wave flumes. In Long Waves Symposium, Thessaloniki, Greece.
- Schäffer, H. A., & Klopman, G. (2000). Review of multidirectional active wave absorption methods. Journal of waterway, port, coastal, and ocean engineering, 126(2), 88-97.
- Schmitt, L., Schmitt, P., Barowski, J., & Hoffmann, M. (2021, February). Stepwise electrostatic actuator system for THz reflect arrays. In ACTUATOR; International Conference and Exhibition on New Actuator Systems and Applications 2021 (pp. 1-4). VDE.
- Spinneken, J., & Swan, C. (2009). Second-order wave maker theory using force-feedback control. Part II: An experimental verification of regular wave generation. Ocean engineering, 36(8), 549-555.
- Spinneken, J., & Swan, C. (2012). The operation of a 3D wave basin in force control. Ocean engineering, 55, 88-100.
- Szmelter-Jarosz, A., Ghahremani-Nahr, J., & Nozari, H. (2021). A neutrosophic fuzzy optimisation model for optimal sustainable closed-loop supply chain network during COVID-19. Journal of Risk and Financial Management, 14(11), 519.
- Timmerberg, S., Börner, T., Shakeri, M., Ghorbani, R., & Alam, M. R. (2015). The "Wave Bridge" for bypassing oceanic wave momentum. Journal of Ocean Engineering and Marine Energy, 1(4), 395-404.
- Van Leer, B. (1979). Towards the ultimate conservative difference scheme. V. A second-order sequel to Godunov's method. Journal of computational Physics, 32(1), 101-136.
- Wu, Y. C. (1988). Plunger-type wavemaker theory. Journal of Hydraulic Research, 26(4), 483-491.
- Wu, Y. C. (1991). Waves generated by a plunger-type wavemaker. Journal of Hydraulic research, 29(6), 851-860.
- Yabe, T., Xiao, F., & Utsumi, T. (2001). The constrained interpolation profile method for multiphase analysis. Journal of Computational physics, 169(2), 556-593.
- Yang, H. Q., Li, M. G., Liu, S. X., & Chen, F. M. (2016). An iterative re-weighted least-squares algorithm for the design of active abso-rbing wavemaker controller. Journal of Hydrodynamics, Ser. B, 28(2), 206-218.